

Facile Hydrothermal Synthesis of Cubic Zinc Ferrite Nanoparticles for Electrochemical Detection of Anti-inflammatory Drug Nimesulide in Biological and Pharmaceutical Sample

Jeyaraman Anupriya¹, Sivakumar Musuvadhi Babulal¹, Tse-Wei Chen^{1,2}, Shen-Ming Chen^{1,*}, Jeyaraj Vinoth Kumar³, Jeong-Won Lee³, Syang-Peng Rwei^{2,4}, Jaysan Yu⁵, Richard Yu⁵, Cheng-Yu Hong¹

¹ Electroanalysis and Bioelectrochemistry Lab, Department of Chemical Engineering and Biotechnology, National Taipei University of Technology, No. 1, Section 3, Chung-Hsiao East Road, Taipei 106, Taiwan, ROC

² Research and Development Center for Smart Textile Technology, National Taipei University of Technology, Taipei 106, Taiwan, ROC.

³ Advanced Nano Surface Engineering Laboratory, Department of Mechanical Engineering, Chosun University, 309, Pilmun-daero, Dong-gu, Gwangju 61452, Republic of Korea.

⁴ Institute of Organic and Polymeric Materials, National Taipei University of Technology, Taiwan

⁵ Well Fore special wire corporation, 10, Tzu-Chiang 7 rd., Chung-Li Industrial Park, Taoyuan, Taiwan

*E-mail: smchen78@ms15.hinet.net

Received: 2 April 2021 / Accepted: 21 May 2021 / Published: 31 May 2021

In this present work, a cubic ZnFe₂O₄ NPs was prepared using facile hydrothermal method. The as-prepared ZnFe₂O₄ NPs capably employed for the detection of anti-inflammatory drug Nimesulide (NS) with the surface modification on the glassy carbon electrode (GCE). The physicochemical properties of as-prepared ZnFe₂O₄ NPs were characterized by XRD, FTIR, FESEM, HR-TEM, and XPS analysis. The electrocatalytic efficiency was investigated through EIS, CV, and DPV electroanalytical techniques. The obtained electroanalysis result demonstrated excellent electrocatalytic activity towards the detection of NS. The constructed ZnFe₂O₄ NPs modified electrode achieved a good linear ranging from 0.001 to 166 μM with a detection limit of 0.006 μM. The calculated analytical sensitivity of the sensor was 0.625 μA μM⁻¹ cm⁻². Moreover, the modified electrode delivers good storage stability, reproducibility and repeatability. Evidently, the proposed sensor manifests the determination of NS in human urine samples and nimesulide tablets for practical applications.

Keywords: ZnFe₂O₄ nanoparticles, Nimesulide, human urine sample, pharmaceutical drug.

1. INTRODUCTION

Nimesulide (4-nitro-2-phenoxyethanesulfonamide) contains a nitroaromatic ring and commonly used as a non-steroidal anti-inflammatory (NSAID) drug, which was selectively used for stopping the prostaglandin production [1]. As compared to NS, the efficacy of NSAIDs such as diclofenac, ibuprofen, and piroxicam possess lower medicinal value. Due to its less acidic (pK_a value= 6.5) nature, which is potentially helpful to reduce gastrointestinal ulcers by ignoring H^+ ions diffusion behind for tissue damage[2]. Furthermore, NS has antipyretic and analgesic properties, which applied in the treatment of rheumatoid arthritis, prostatovesiculitis, osteoarthritis disorder [3][4]. Subsequently, NS largely appears as an ecological contaminant in hospital effluent and local sewage water. The contaminant level of NS was found to be $9.731 \mu\text{g L}^{-1}$ in the wastewater treatment unit, that was reported by Papageorgiou *et al* research group [5]. Therefore, the regular monitoring and detection of NS in the environmental ecosystem is an important concern. Researchers are urged to develop a novel, simple and economical sensors with high consistency and sensitivity for the detection of NS. Some past literature studies suggest that the NS determination has been utilized including chromatography HPLC, UV, thin-layer chromatographic technique (TLC), infrared (IR) spectrophotometry, capillary zone electrophoresis (CZE), and micellar electrokinetic capillary chromatography (MEKC) [6][7][8]. These conventional methods have some disadvantages. These aforementioned methods have complex analysis measures, time-consuming, trained person need for experimental operation, low sensitivity toward the detection of analyte and involve with high-cost instruments. Under other condition, Cyclic voltammetry offers robust analytical techniques with benefits of instrumental simplicity, low cost and transferability. Subsequently, most electro-analytical techniques are selective to the determination of analyte and accomplished with high sensitivity, fast measurements over a wide linear range [9–13], which involves simple sample preparation method and specified the fact that NS is electroactive. The electrochemical methods are best known as viable and better alternatives for the determination of NS when compared to the other methods.

Metal oxide nanomaterials have been widely studied as a sensing platforms due to their improved analytical fulfilment. Especially, $M\text{Fe}_2\text{O}_4$ (metal ferrites), here M could be Zn [14], Cu [15], Co[16] and Mn [17] as these are widespread magnetic materials applied in sensors, analytical application, biomedicine and drug delivery system. The spinel ferrites ($M\text{Fe}_2\text{O}_4$) are prepared by using sol-gel [18], co-precipitation [19], ball milling method [20], solvothermal reflux and hydrothermal method [21]. ZnFe_2O_4 is one of the most important ferrite binary oxides with the ferromagnetic property. The quality of the spinel ferrite depends on the preparation and sinter condition. Because of biocompatibility, low toxicity electrical properties and high adsorption abilities of zinc ferrite nanoparticles, it has been extensively used in the electrochemical sensor and biosensor field [22–26]. For an instance, Lv *et al.*, [27] reported the Sb doped ZnFe_2O_4 macroporous sphere nanoparticles modified electrode used for sensing the N-butanol through the gas sensor. Neravathu *et al.*, [28] demonstrated that $\text{ZnFe}_2\text{O}_4/\alpha\text{-Fe}_2\text{O}_3$ implanted graphene nanocomposite used for detection of glucose. Zheng *et al.*, [29] confirmed that $\text{ZnFe}_2\text{O}_4/\text{ZnO}$ gas sensor senses trimethylamine sensing with excellent selectivity and high response. Huang *et al.*, [30] started to synthesize the optimized ordered mesoporous ZnFe_2O_4 via the facile nano casting method. The synthesized electrode shows a wide linear range and fast response to dopamine

oxidation. Ning *et al.* [31] established a graphene sheet supported Pd and ZnFe₂O₄ modified electrode used to detect hydrogen peroxide sensor.

This work aimed to characterize the surface feature of the ZnFe₂O₄ nanoparticles (denoted as ZnFe₂O₄ NPs) and to determine the electrocatalytic activity of the ZnFe₂O₄ NPs modified GCE. was used for voltammetric sensing of NS. The ZnFe₂O₄ NPs characterized by XRD, FTIR, XPS, FESEM, and HRTEM. The as-synthesized ZnFe₂O₄ NPs modified glassy carbon employed for building an electrode for the analysis of NS in biological and pharmaceutical samples. This is the first report for the detection of NS through the electrochemical sensor using ZnFe₂O₄ NPs. Also, ZnFe₂O₄ NPs has been used for real-time monitoring of NS tablet and human urine sample investigated.

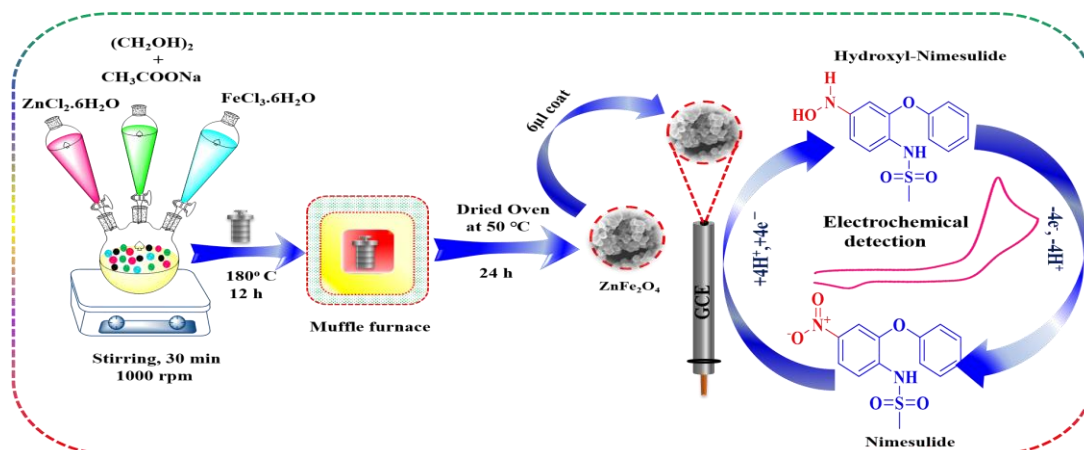
2. MATERIAL AND METHODS

2.1 Chemicals

The analytical grade of Zinc chloride hexahydrate ZnCl₂.6H₂O, Ferric chloride hexahydrate FeCl₃.6H₂O and ethylene glycol (99% pure) was purchased from Sigma Aldrich. Sodium dihydrogen phosphate monohydrate (NaH₂PO₄.H₂O), sodium phosphate dibasic anhydrous (Na₂HPO₄), hydrochloric acid, NaOH were purchased from Sigma Aldrich chemical reagent Co. (MO, USA). All reagent were of analytical grade and used without further purification.

2.2 Hydrothermal synthesis of the ZnFe₂O₄ nanoparticle

The pristine ZnFe₂O₄ NPs was prepared by a hydrothermal route using the previously reported method with some modification [32]. Initially, the precursor solution of zinc chloride 0.5 M (0.6 g) and ferric chloride 0.05 M (0.13 g) was dissolved in 20 mL deionized water separately. Afterwards, each solution was mixed one by one under continuous magnetic stirring condition. Then 5 mL of ethylene glycol and 5 mL of sodium acetate was mixed into the above solution. After added ethylene glycol the brown colour colloidal suspension was formed and stirring continued for half an hour until the homogeneous solution formed. Then the obtained homogeneous solution was transferred into a Teflon-lined stainless steel autoclave with a capacity of about 50 mL. The autoclave was sealed and maintained at 180 °C for 12 h after cooled at ambient temperature. Finally, the obtained brown precipitate was washed and centrifuged many times using DI water and ethanol then dried in an oven at 50 °C for 24 h. The synthesis and fabrication of the ZnFe₂O₄ NPs were depicted as shown in Scheme 1.



Scheme 1. The schematic diagram for the synthesis procedure and fabrication of the ZnFe_2O_4 NPs and their electrochemical mechanism.

2.3 Characterization and instrumentation

The crystallographic structure of the pristine ZnFe_2O_4 NPs was identified by powder X-ray diffraction (PXRD) using radiation from a $\text{Cu K}\alpha$ target ($\lambda = 0.1541 \text{ nm}$) at a scan rate of 2° min^{-1} . The morphology and size of the ZnFe_2O_4 nanoparticle were characterized using field emission scanning electron microscopy (FESEM, quanta 250, FEG, Hitachi, Japan operated at 15 kV) and High-resolution transmission electron microscopy ((HRTEM, JEOL 2100F) techniques. The existing functional groups examined by Fourier Transform - Infrared spectroscopy (JASCO, CHI 1000C, FT-IR-6600 spectrometer). The X-ray photoelectron spectroscopy (XPS, Thermo ESCALAB 250) were performed by using Thermo ESCALAB 250 instrument. Electrochemical chemical measurements were performed with electrochemical impedance spectroscopy (EIS-IM6ex ZAHNER (Kronach, Germany), cyclic voltammetry (CV-CHIInstrument-1205B) and differential pulse voltammetry (DPV) (CH Instrument 750A). The conventional three-electrode system performed on glassy carbon electrode as a working electrode (GCE surface area = 0.071 cm^2), platinum wire (0.5 mm diameter) as a counter electrode and Ag/AgCl (saturated 3.0 M KCl) electrode as a reference electrode.

2.4 Fabrication of ZnFe_2O_4 NPs modified GCE

Initially, the blank surface of the glassy carbon electrode (GCE) was polishing with the help of $0.05 \mu\text{M}$ alumina slurry, polishing pad, water and ethanol. Then GCE was dried at ambient temperature for further uses. The 5 mg of ZnFe_2O_4 NPs were dispersed in 1 mL of Millipore Q-water, then an ultrasonic agitation 30 mins to make a dispersion. Thus, obtained dispersion at $6 \mu\text{L}$ (optimized concentration) homogeneously dropped cast onto the mirror surface of the GCE and dried at 50°C hot air oven. The acquired ZnFe_2O_4 NPs modified GCE was employed for further electrochemical analysis.

3. RESULT AND DISCUSSION

The crystallinity nature of the as-prepared pristine ZnFe_2O_4 NPs was confirmed by the x-ray diffraction pattern. Fig. 1(A) shows the peak at 2θ values of 18.1° , 29.9° , 35.2° , 36.8° , 42.8° , 53.1° , 56.6° and 73.5° respectively, which are attributed to the corresponding planes (111), (220), (311), (400), (422), (511), (440), (620) and (533) of the ZnFe_2O_4 in the cubic structure with Fd-3m space group and JCPDS 01-082-1042 confirm the formation of the ZnFe_2O_4 pure phase [32]. No additional peak was found in ZnFe_2O_4 NPs indicating high purity and high crystallinity. The average crystallite size was calculated by applying high intensity of ZnFe_2O_4 NPs diffraction peak using Scherrer's formula

$$D = (K\lambda)/\beta\cos\theta \quad (1)$$

Where K indicates the geometry dependent constant on the unit cell which is 0.9, the value of D is the crystallite size, λ is the wavelength of radiated X-ray (in Å), θ corresponding to the Bragg diffraction angle, β is full width at half maximum after correction for instrument error (in radian). The Scherrer formula derived the calculated average crystallite size is 9.64 nm. Fourier transform infrared spectroscopy (FT-IR) is a crucial tool used to characterize different branches of singular resonant vibration mode of molecules. It can reveal those constituting elements and their bonding arrangement. Besides, it enables in-situ analysis of interfaces to investigate the surface adsorption of the functional groups on the nanoparticle. Fig. 1(B) portrays the FT-IR spectrum of the ZnFe_2O_4 NPs in the range of $4000\text{-}400\text{ cm}^{-1}$. The FT-IR spectrum was revealed mainly in two broad regions, the first one is metal oxide lattice vibration occurred at higher energy region and lower energy region has the organic functional group. The as-prepared ZnFe_2O_4 NPs shows a transmittance band at higher energy 543 cm^{-1} , which is corresponds to the intrinsic stretching vibration of the metal tetrahedral (Zn-O) site [32]. Moreover, metal octahedral stretching vibration has displayed at lower energy 435 cm^{-1} . The peak bands at 1081 cm^{-1} and 2925 cm^{-1} are attributed to the stretching of the ether groups and absorption of alkyl (R-CH_2) stretching modes that appeared on the surface of the ZnFe_2O_4 NPs. In addition, the rational absorption peak at 1650 cm^{-1} and 3432 cm^{-1} are characteristics of the O-H stretching mode of absorbed water molecules on the surface of the prepared nanoparticle [32,33]. The above all corresponding peaks are confirmed that as prepared ZnFe_2O_4 NPs and presence of ethylene glycol on the surface.

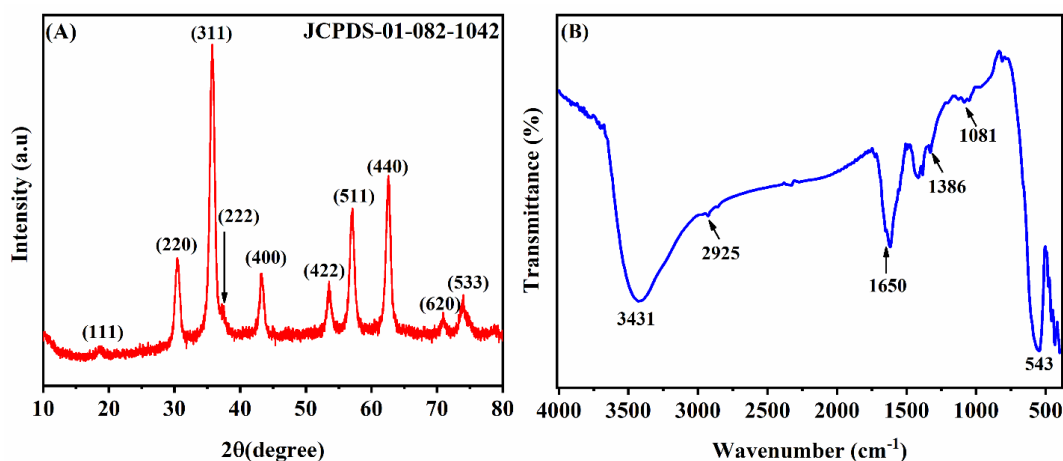


Figure 1. (A) The XRD pattern of the pristine ZnFe_2O_4 NPs, (B) FT-IR spectrum of the ZnFe_2O_4 NPs.

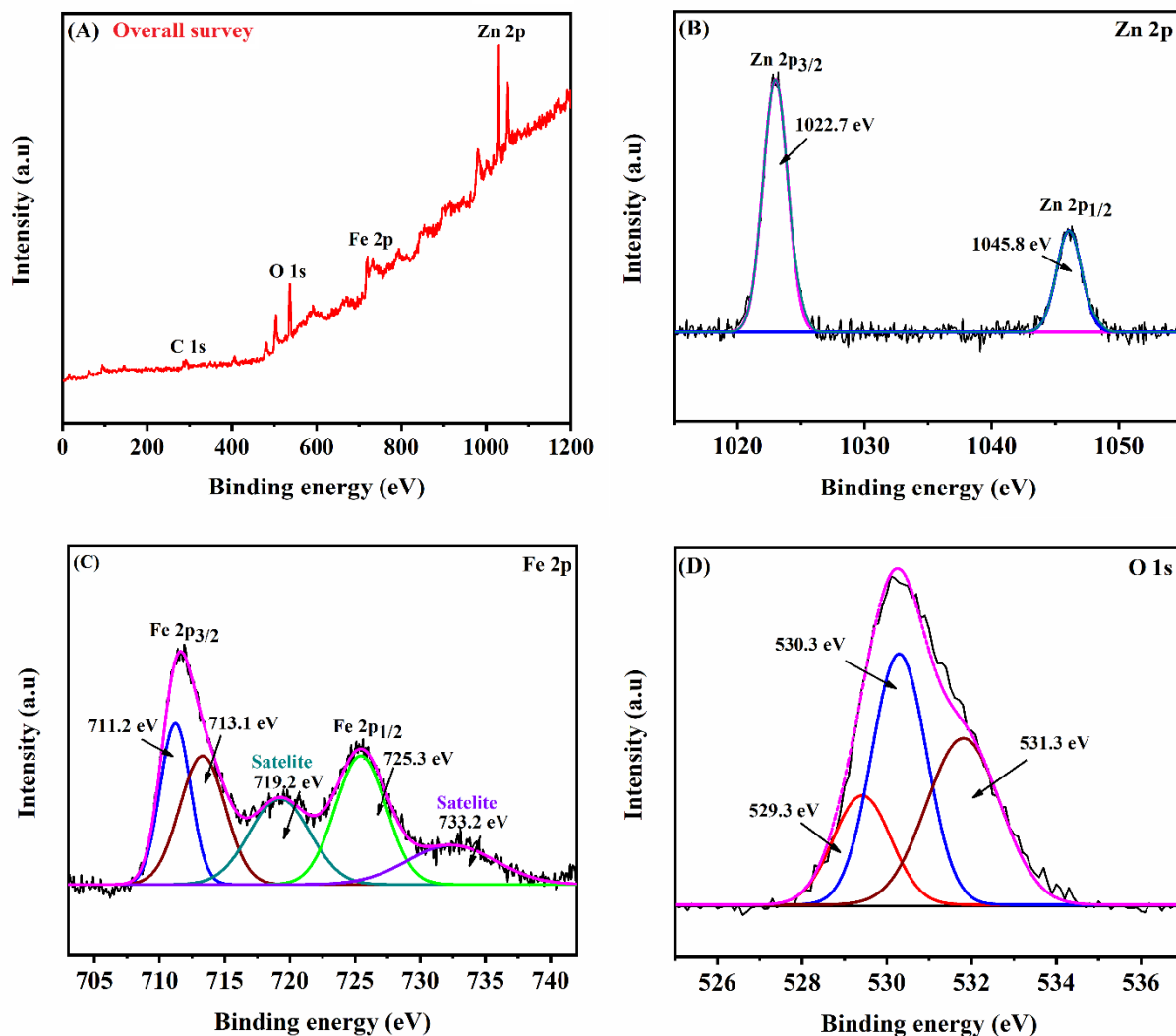


Figure 2. (A) Full XPS spectrum of ZnFe₂O₄ NPs. (B-D) The high-resolution XPS spectra of Zn 2p, Fe 2p, O 1s at ZnFe₂O₄ NPs.

The photoelectron spectrum has reproduced the electronic structure of an element quite accurately [34]. The identification of elemental composition and oxidation states of the ZnFe₂O₄ NPs were scrutinized by X-ray photoelectron spectroscopy (XPS) analysis. Fig 2(a) shows the overall survey spectrum of Zn, Fe, O elements that existed in the ZnFe₂O₄ NPs. Fig. 2(b-d) displays Zn-2p, Fe-2p, O-1s spectra of the ZnFe₂O₄ NPs respectively.

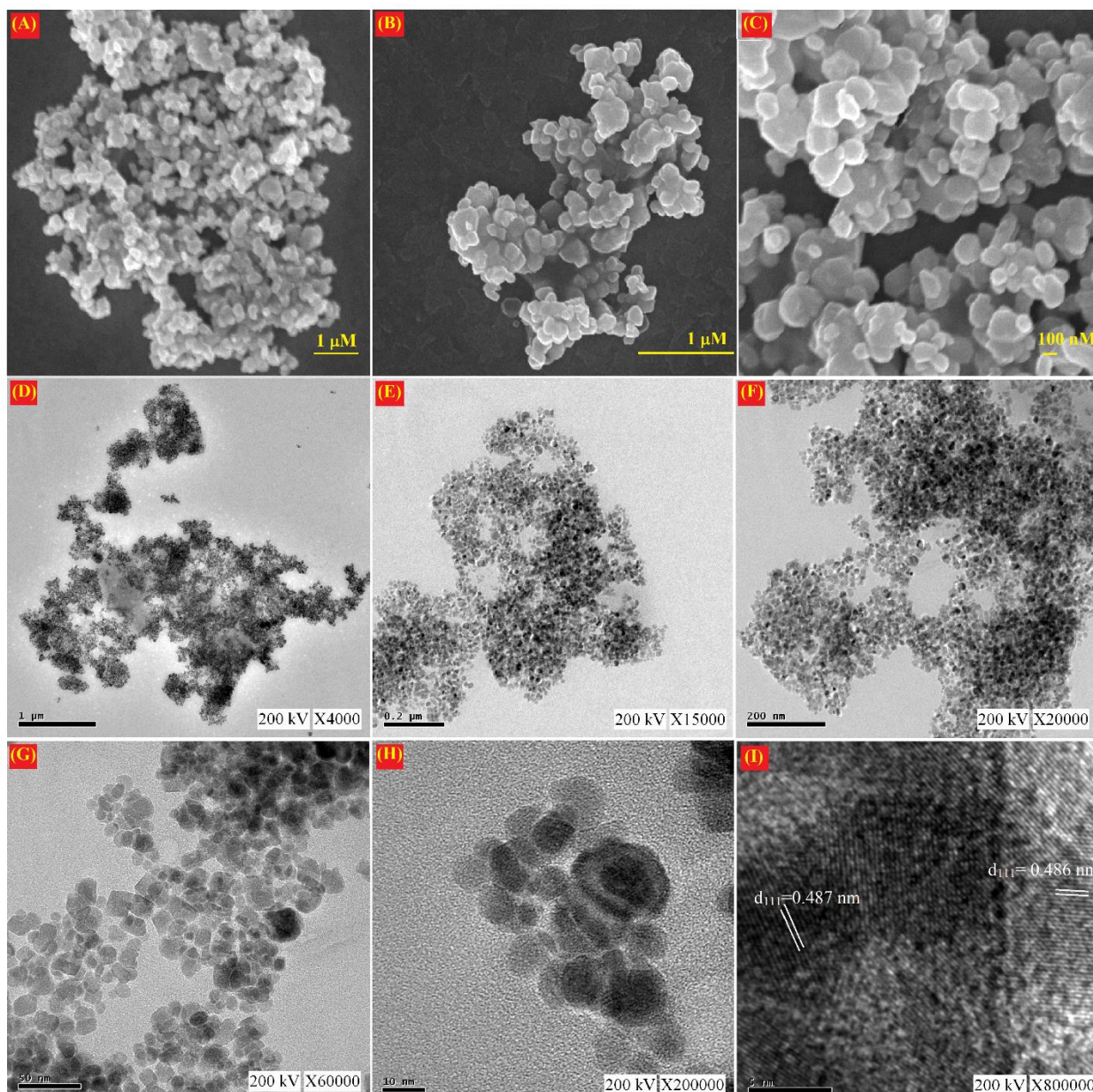


Figure 3. (A-C) FE-SEM images of the ZnFe_2O_4 NPs, (D-I) HR-TEM images of the ZnFe_2O_4 NPs.

The two main peaks of $\text{Zn } 2p_{3/2}$ and $\text{Zn } 2p_{1/2}$ are observed at the binding energy of 1022.7 eV, and 1045.8 eV respectively [35], as shown in Fig. 2(b). The obtained binding energy values revealed that Zn exists mainly in the +2-oxidation state of the as-prepared ZnFe_2O_4 NPs. Four signals emerged in the high-resolution spectrum of Fe 2p as displayed in Fig. 2(C). The main peaks of Fe $2p_{3/2}$ and Fe $2p_{1/2}$ binding energy are located at 711 eV, 713 eV and 725.3 eV respectively. These values are confirmed that the oxidation state of Fe^{2+} and Fe^{3+} featured in the octahedral and tetrahedral site of the prepared product. Also, the binding energy value of 719.2 eV and 733.2 eV were ascribed to their satellite peaks [36–38]. The O-1s spectra (Fig. 2D) displays a significant peak at 529.3 eV, 530.3 eV and 531.3 eV for lattice oxygen connected with Zn and Fe (represent as Zn-O and Fe-O) respectively. From the XPS results, we confirm that all elements are present in the ZnFe_2O_4 NPs [39].

The ZnFe_2O_4 NPs was synthesized through the hydrothermal route. The crystalline morphology and shape of the ZnFe_2O_4 NPs were confirmed by FE-SEM analysis. As shown in Fig. 3(A-C), the two different magnification of ZnFe_2O_4 NPs clearly illustrates that the uniform dispersed spherical morphology. Especially, the particle size and cubic structure of the nanoparticle were caused by the synthesis method. The obtained ZnFe_2O_4 NPs has cubical morphology with average particle size in the ranges of 10-60 nm. The hydrothermal route synthesized nanoparticle was exhibited feature structures with higher crystallinity, large surface area and good electrocatalytic activity. Each of these significant properties needs to enhance the electron transfer rate for sensing application [39]. Further, the analysis of HR-TEM of as-prepared ZnFe_2O_4 NPs with different magnification views were shown in Fig. 3(D-H). The prepared ZnFe_2O_4 NPs were nearly cubical and uniformly distributed. The average size diameter of the single ZnFe_2O_4 NPs was found in the range of 10 nm (< 5 nm). The as-prepared ZnFe_2O_4 NPs displayed a clear interplanar distance of 0.486 nm and 0.487 nm, corresponding to the (111) crystal plane (Fig. 3I) of the cubic structure of the synthesized nanoparticle [38].

3.2. Electrochemical characterization of ZnFe_2O_4 NPs modified GCE

EIS is the specific tool to investigate the charge transfer resistance and kinetics mechanism between constructed ZnFe_2O_4 NPs electrode and electrolyte interface. Since the EIS instrument was active to display and examine the impedance changes at the electrode-electrolyte interfacial region. This experiment was carried out in 0.1 M KCl containing a stoichiometric ratio of 5 mM $[\text{Fe}(\text{CN})_6]^{3-/4-}$ system at a frequency range from 1 kHz to 200 mHz and the outcomes were obtained in the form of a Nyquist plot. Fig. 4A demonstrates the EIS spectra of an unfabricated electrode and constructed ZnFe_2O_4 NPs electrode. According to the Nyquist plot, it consists of two segments, where Z was denoted as a real part and Z' was considered as an imaginary part of the impedance. As shown in the plot, the semicircular segment at higher frequency was manifested as charge transfer resistance and the linear segment at lower frequency was denoted as diffusion region. Fig. 4A inset designates the facile electrochemical interface of the Randles circuit model. Where R_s denotes active electrolyte resistance, C_{dl} denotes double-layer capacitance, Z_w denotes Warburg diffusion coefficient and R_{ct} denotes charge transfer resistance. The measured R_{ct} values at the semicircular curve of bare GCE and constructed ZnFe_2O_4 NPs are 136 Ω and 3720 Ω respectively. The constructed ZnFe_2O_4 NPs was depicted 27.35-fold higher charge transfer resistance than bare GCE, which confirms the successful construction of ZnFe_2O_4 NPs on GCE. The aforementioned results concluded that the ZnFe_2O_4 NPs/GCE exhibits a higher R_{ct} value owing to four following reasons: (i) The interaction between cations and anions (Fe^{3+} , Zn^{2+} , and O^{2-} anion); (ii) The interaction between the spin-polarized electrons of Fe^{3+} and conductive electrons; (iii) Interaction between metal ions and metal oxide; (iv) The poor electrical conductivity of ZnFe_2O_4 NPs [40–42]. Moreover, the above-mentioned causes were the fabricated ZnFe_2O_4 NPs electrode manifested higher charge transfer resistance than bare GCE.

3.3. Electrochemical reduction behaviour of towards Nimesulide

The cyclic voltammetry (CV) was primarily attained to conform to the electrocatalytic detection performance of fabricated electrodes in the presence of NS. This experiment was carried out in N_2 purged 0.1 M PBS (pH-7) with 100 μ M of NS and scan amplitude, potential windows followed by 50 mV/s, 0.2 to -0.8 V.

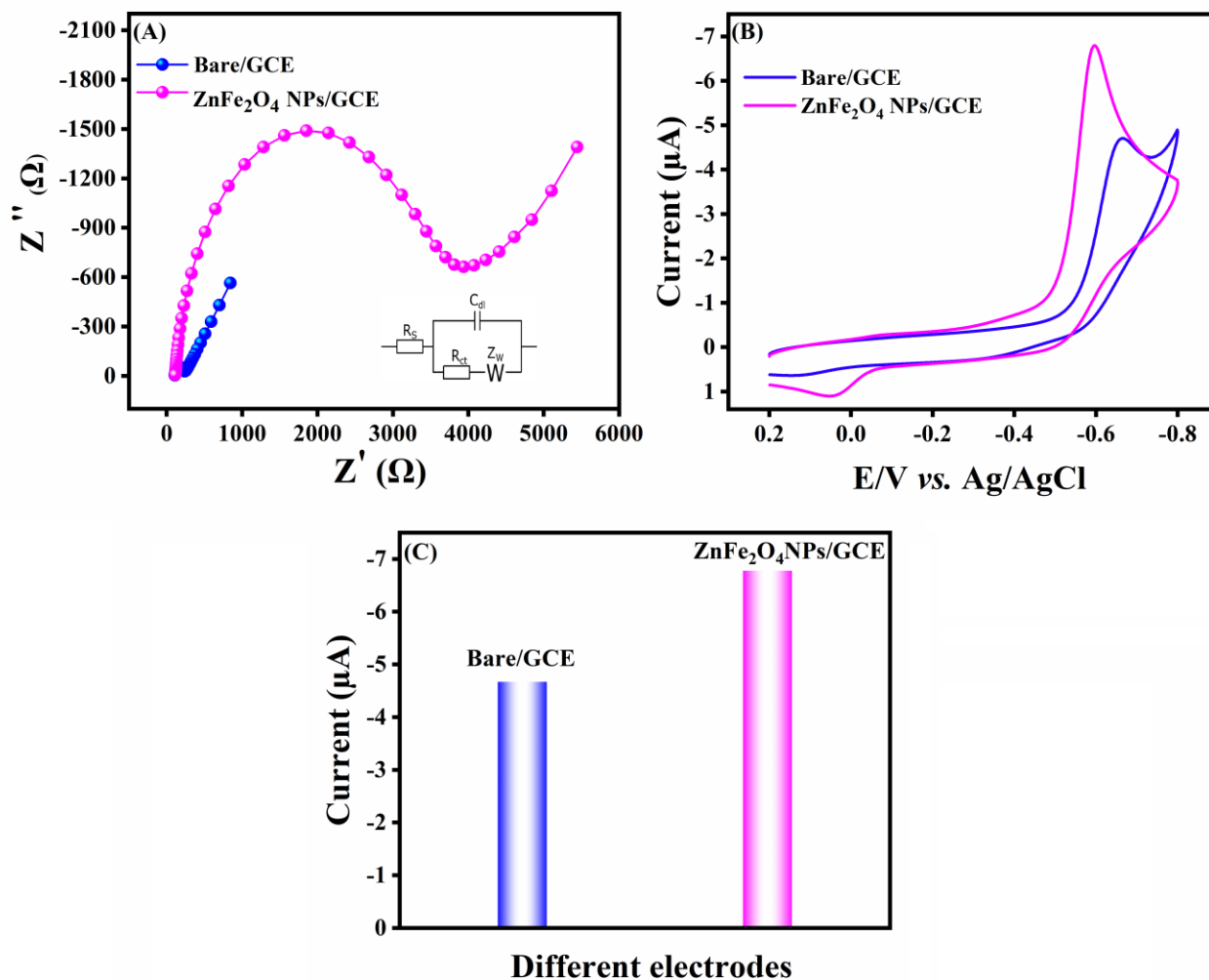
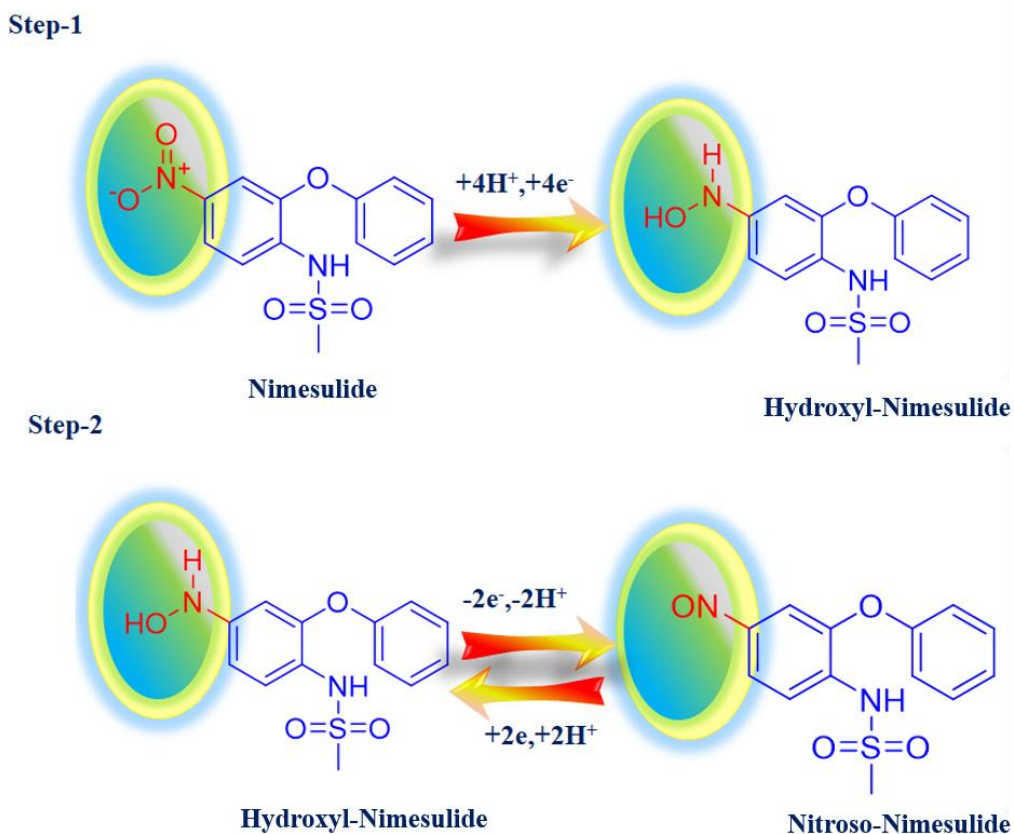


Figure 4. (A) EIS Nyquist curve for bare GCE and $ZnFe_2O_4$ NPs/GCE (inset: Randles equivalent circuit model). (B) CVs response of bare GCE and $ZnFe_2O_4$ NPs/GCE in the presence of 100 μ M of NS in 0.1 M of PBS (pH-7) solution with a scan rate at 50 mV/s and (C) Corresponding bar diagram of bare GCE, $ZnFe_2O_4$ NPs/GCE.

Moreover, the outcome of this experiment, bare GCE shows a very feeble reduction current at -4.6 μ A with the corresponding reduction peak potential at -0.66 V, owing to the inability to catalyze the redox reaction of NS and the predominant oxidation peaks are non-insurable. Further, the fabricated $ZnFe_2O_4$ NPs/GCE exhibits cathodic current at -6.75 μ A with a corresponding cathodic potential value

at -0.59 V and a small anodic current appeared at 1 μ A with corresponding peak potential at 0.07 V shows in Fig. 4B.



Scheme 2. Electrocatalytic reduction mechanism of NS.

From this result, the fabricated ZnFe_2O_4 NPs/GCE exhibit an incredible electrocatalytic performance, a high reduction peak current and it exhibit excellent electrocatalytic ability towards NS, owing to the electrocatalytic irreversible reaction of NS containing nitro group ($-\text{NO}_2$) was directly reduced to form hydroxyl-1-nimesulide ($-\text{NHOH}$) in the 1st step. Here, the reduction mechanism involved 4-electron and 4-protons. In furtherly, the reversible mechanism has occurred in the hydroxyl-1-nimesulide ($-\text{NHOH}$) was converted into nitroso Nimesulide. This electrochemical reduction mechanism of NS was illustrated in Scheme 2. Moreover, the corresponding bar diagram for bare GCE and fabricated ZnFe_2O_4 NPs electrodes was exposed in Fig. 4C. This result demonstrated that the constructed ZnFe_2O_4 NPs exhibit an efficient capability to sense NS and a complete electrochemical reduction mechanism occurred in NS. Furthermore, other electrochemical parameters also influence the electrochemical activity of NS such as the effect of different pH, the effect of analyte addition, and change in scan rate are discussed below.

3.4. Influence of different pH

The electrochemical reduction of NS affecting one of the leading factors was different pH. Besides, necessary to study the protonation and deprotonation mechanism of the newly constructed ZnFe_2O_4 sensor towards NS. This study was conducted via a CV experiment in 100 μM of NS with the pH solution was changed from 3 to 11 (pH 3, 5, 7, 9 and 11) was shown in Fig. 5A. As a result, in pH to 3 to 7, the potential was a shift toward negatively and the current correspondingly increased. Consequently, the electrochemical reduction of NS was converted into hydroxylamine group (NHOH) in 1st step of stable reduction was happened. Subsequently, in pH 9 and 11 the potential shift was towards negatively and the current was reduced. This is owing to the complete utilization of hydroxylamine, further converted into the nitroso amine in the 2nd step irreversible process was happened. Besides, the protonation and deprotonation equally arisen for this reduction mechanism of NS. Finally, the maximized sensitive current (-6.08 μA) was observed in the pH-7 solution. The number of electrons and protons that are equal participants in the electrochemical reactions, were calculated from the Nernst equation [43].

$$dE_{pc} / dpH = -2.303mRT/nF \quad (2)$$

As a result, to obtained slope value was 53 mV/pH (m/n) more or less equal to the theoretical value 59 mV/pH (m/n). This indicates an equal number of electron and protons have participated in this reaction was illustrated in scheme-2. A corresponding linear diagram of different pH vs current vs potential was shown in Fig. 5B. The relative static equation of potential vs different pH was exhibit $E_{pc} = -0.053x - 0.372$ and relative correlation co-efficient $R^2 = 0.968$. This indicates an increased pH the potential shift was increased linearly. It concludes that the pH-7 solution was finest for the further all electrochemical reduction process and conversion of NS into hydroxylamine was a more stable product and the electrochemical reduction of NS affecting one of the promising factors was a change in pH.

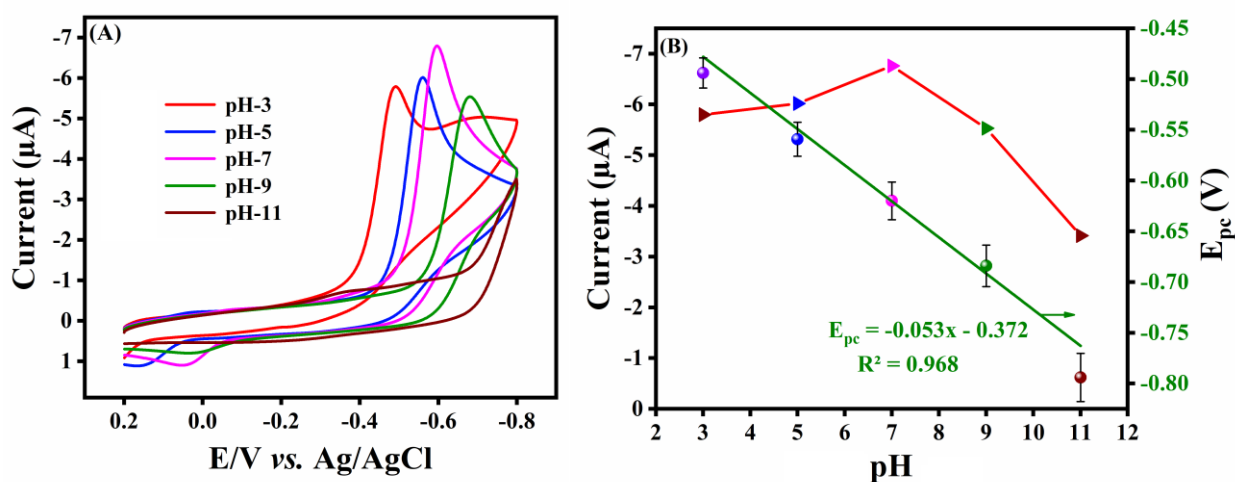


Figure 5. (A) CV response of ZnFe_2O_4 NPs/GCE at a sweep rate at 50 mV/s in various PBS solution pH (3,5,7,9 and 11) with 100 μM of NS. (B) Corresponding linear diagram of different pH vs current (μA) vs potential (V). (C) CV performance of ZnFe_2O_4 NPs/GCE with the addition of NS (75–175 μM) in 0.1 M PBS solution with scan rate at 50 mV/s (D) Corresponding, calibration curve between the concentration of an analyte (NS) vs cathodic current (μA).

3.5. Influence of NS concentration

The electrochemical activity of NS over the fabricated ZnFe₂O₄ NPs/GCE carry out in a CV, the NS concentration was changed from 75 to 175 μM , in 0.1 M of N₂ purged PBS solution with scan rate and potential windows were followed by 50 mV/s and 0.2 to -0.8 V. At this point, observed the concentration of NS increased and current increased linearly as shown in Fig. 6A. Owing to the reduction mechanism of NS into hydroxylamine. At the same time, the small anodic peak was observed at 0.07 V. This was Owing to the reversible mechanism of hydroxyl-1-nimesulide ((-NHOH) was converted into nitroso Nimesulide. Furthermore, the addition of analyte the current was increased linearly as well as the potential shifted towards negatively. Fig. 6B expresses the linear relation between current and analyte addition. The corresponding linear statics equation $y = -0.041x - 2.84$ and correlation coefficient $R^2 = 0.991$. It reveals that, the good linear relation between current and analyte addition.

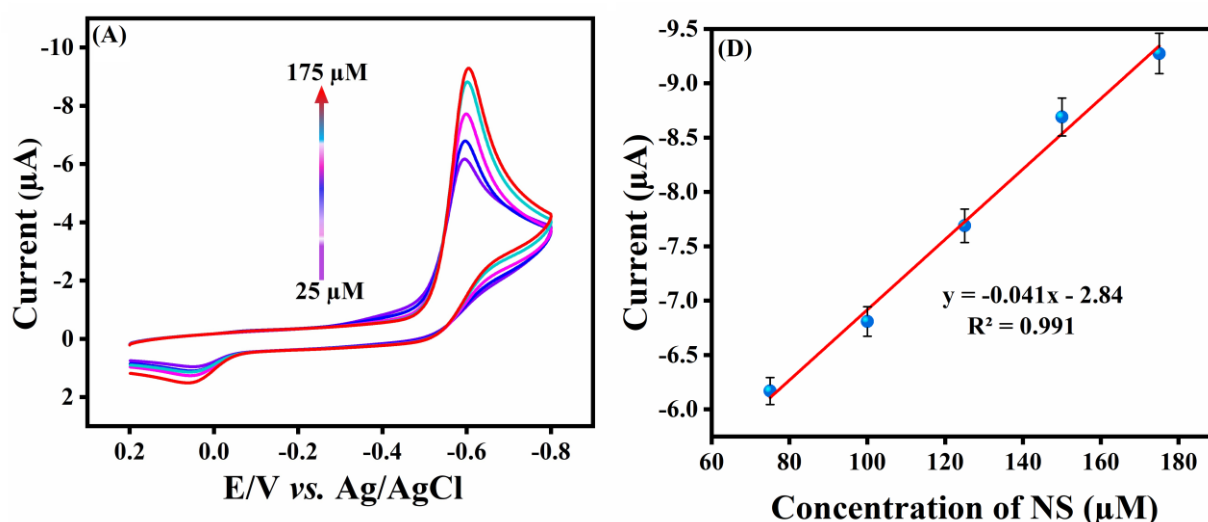


Figure 6. (A) CV performance of ZnFe₂O₄ NPs/GCE with the addition of NS (75 to 175 μM), (B) Corresponding, calibration curve between the concentration of an analyte (NS) and cathodic current (μA).

3.6. Effect of scan rate

The effect of scan rate was the main important factor to affect the electrocatalytic reduction of NS. These studies were carried out in CV investigations N₂ purged 0.1 M of PBS solution with the scan rate changed from 20 mV/s to 200 mV/s and the amount of NS added at 100 μM with the potential window were followed from 0.2 to -0.8 V. Fig. 7A shows, an increasing scan rate the cathodic current was too increased. Owing to, an increasing scan rate the electrochemical reaction time was shortened as a consequence cathodic current was increased. Meanwhile, a high scan rate causes electrochemical reaction time was increased and current linearly increased. Meanwhile, with an increasing scan rate, the potential was a shift towards negatively. Fig. 7B represents the calibration curve between the cathodic

current (*vs*) square root of scan rate. It reveals that a good linear agreement with a current *vs* square root of scan rate. This corresponding, the linear statics equation presumed through $y = -0.797x - 0.308$ and relative correlation co-efficient $R^2 = 0.987$.

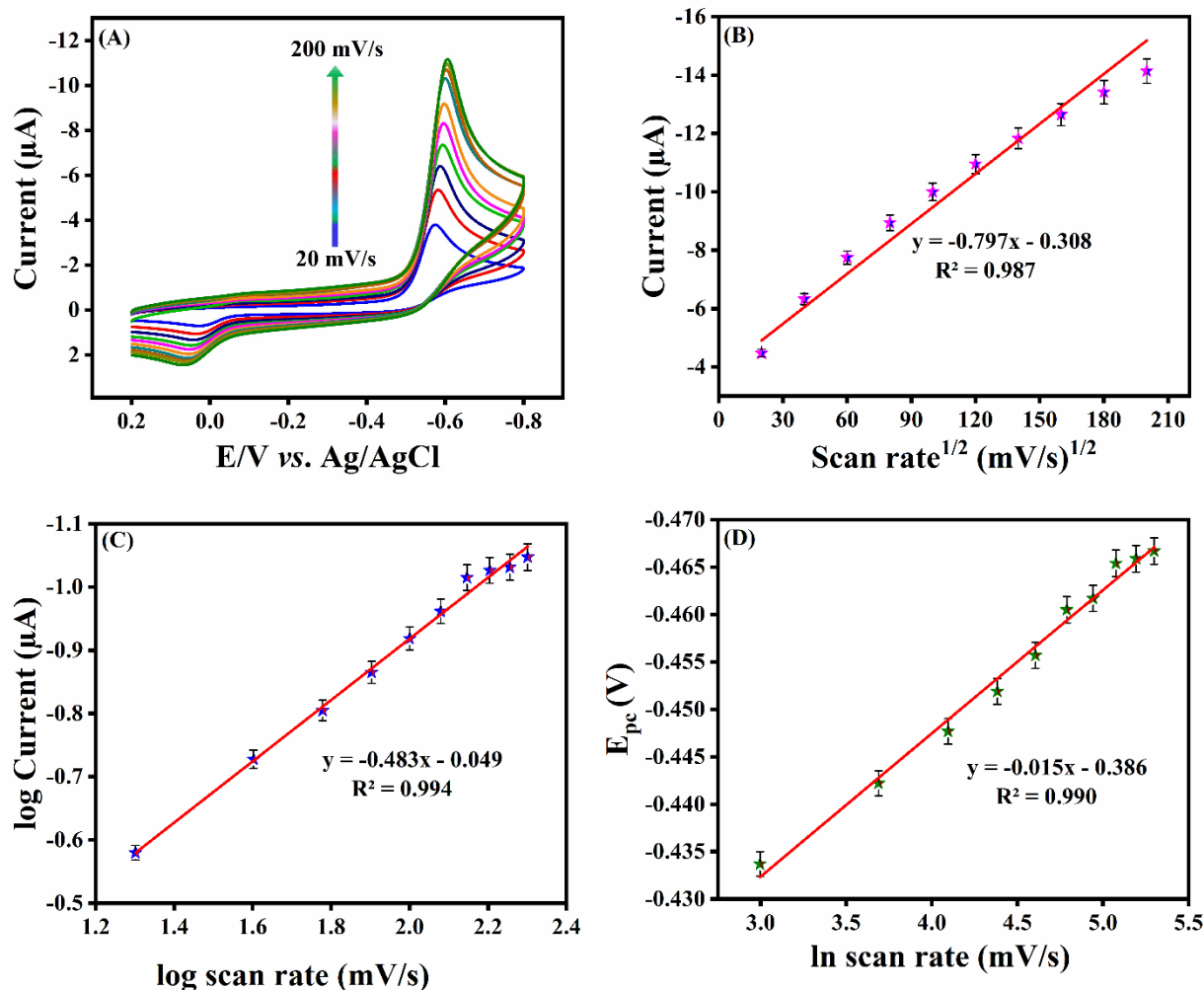


Figure 7. (A) CV current response of ZnFe₂O₄ NPs/GCE in the presence of 0.1M of PBS solution contains 100 μM of NS and scan rate changed from 20-200 mV/s. (B) Calibration curve between current (μA) *vs* square root of scan rate (mV/s)^{1/2}. (C) Calibration curve between the log of current (μA) *vs* log of scan rate (v). (D) Calibration curve between potential (V) *vs* ln of scan rate (v).

This reveals that the electrochemical reduction reaction of NS on ZnFe₂O₄ NPs/GCE was a diffusion-controlled process. However, a linear correlation was detected between log scan rate *vs* log cathodic current. The observed linear statics equation $y = -0.486x - 0.049$, $R^2 = 0.994$ shown in Figure 7C. The aforementioned, observed ideals are confirmed the electrochemical reduction reaction was a diffusion-controlled process and the electrochemical reaction was a time-dependent process. Additionally, some other parameters such as charge transfer coefficient (α) and standard electron transfer

rate (k'_s) correspondingly influenced the kinetics of electrochemical reduction. Besides, such parameters are described in Laviron's equation. Moreover, the linear regression plot between \ln scan rate (v) potential was exposed in Fig. 7D. Corresponding linear regression equation and relative coefficient specified in $y = -0.015x - 0.386$; $R^2 = 0.990$. From this plot, the slope value was calculated and substituted in Laviron's equation [44].

$$E_{pc} = E^0 + (RT/\alpha nF) \ln(RTK_s/\alpha nF) + (RT/\alpha nF) \ln v \quad (3)$$

Where α was denoted as charge transfer coefficient and v was denoted as scan rate of the reduction reaction. R and T were usual parameters of gas constant ($8.314 \text{ JK}^{-1}\text{mol}^{-1}$) and room temperature (298K). n is the number of electrons are participated in this reduction reaction ($4e^-$). F was denoted as a Faraday's constant (96485.3 C/mol). The charge transfers value (α) and standard electron transfer coefficient (k'_s) were calculated to be 0.5 and $1.36 \times 10^{-4} \text{ cm}^2 \text{ s}^{-1}$ [45].

3.7. Electrochemical reduction of NS via DPV

The LOD and sensitivity of the constructed ZnFe_2O_4 NPs/GCE sensor towards NS were investigated via DPV analysis. These studies were carried out in N_2 purged 0.1 M of PBS solution with a concentration of analyte added from $0.1 \mu\text{M}$ to $166 \mu\text{M}$ and the potential range was fixed from 0.2 to -0.8 V . As a result, an increasing concentration of NS the current increased linearly. Moreover, the current *vs* addition of analyte was shown in Fig. 8A.

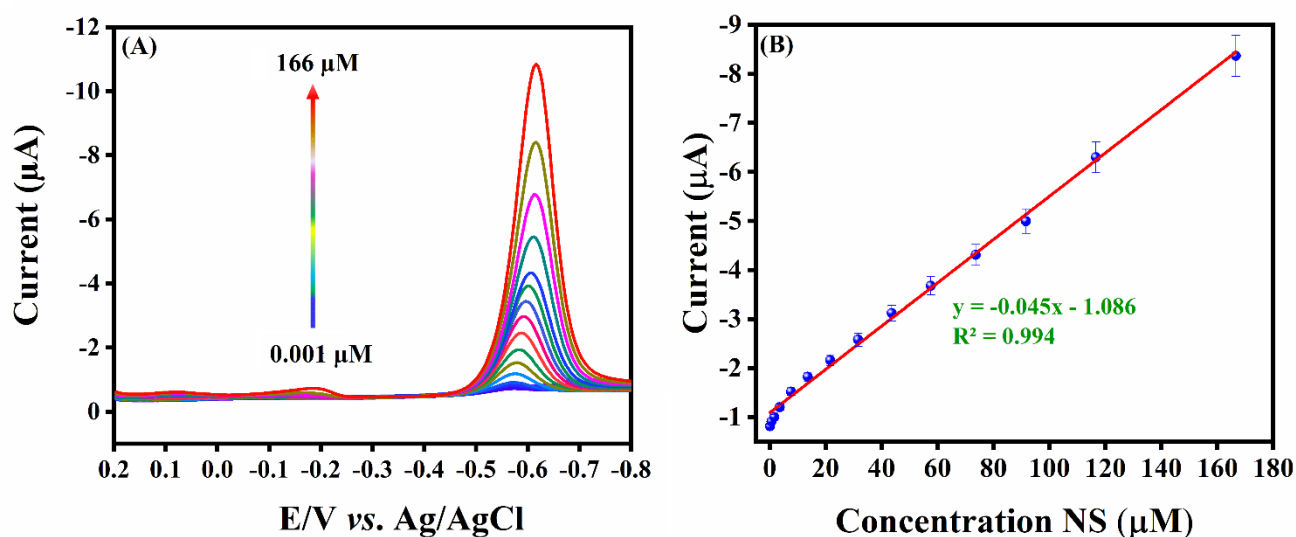


Figure 8. (A) DPV current response of ZnFe_2O_4 NPs/GCE towards NS addition 0.1 to $166 \mu\text{M}$ in N_2 purged 0.1 M of PBS solution. (B) The linear correlation curve between current (μA) *vs* concentration of NS (μM).

This indicates the complete utilization of NS on ZnFe_2O_4 NPs/GCE with the high linear range was achieved to be 0.01 – $166 \mu\text{M}$. Fig. 8B illustrates the linear correlation curve between reduction current *vs* concentration of an analyte. Further, the linear regression equation obtained $y = -0.045x - 1.086$ and the relative correlation coefficient, $R^2 = 0.994$. The aforementioned values are, indicate the

good linearity between current and analyte addition. From this linear curve, the limit of detection ($S/N=3$) and the sensitivity (S) were calculated to be $0.006 \mu\text{M}$ and $0.625 \mu\text{A} \mu\text{M}^{-1} \text{cm}^{-2}$. Furtherly, the constructed sensor sensitivity and the linear range were correlated with the previous reports in Table 1. This indicates the good linear range, high sensitivity, and trace level detection was an exhibit by the proposed sensor.

Table 1. Comparison of other fabricated electrodes for the determination of NS.

Modified Electrodes	Linear range (μM)	Limit of detection (μM)	Reference
Cysteic acid/CNTs/GCE	0.1-10	0.05	[46]
MWCNTs/GCE	0.3-65	0.16	[47]
Glassy Carbon electrode	0.4-50	0.032	[48]
Fe_2O_3 magnetic nanoparticle/GCE	2.6-1000	0.13	[49]
ZnFe_2O_4 NPs/GCE	0.001-166	0.006	This Work

3.8. Selectivity, repeatability, reproducibility and storage stability.

Selectivity is an important factor for newly constructed electrochemical sensors. Fig. 9A represents the DPV obtained polarography for selectivity study. Moreover, this experiment was carryout in N_2 purged 0.1 M of PBS solution with anti-interference property were checked by using various metals, biomolecules, and nitro compounds. Fig. 9B exposed the bar diagram of current vs various foreign molecules such as calcium (Ca^{2+}), magnesium (Mg^{2+}), dopamine (Dop), uric acid (UA), nitroaniline (NA), nitrofurazone (FZ), nitrofurantoin (NTF), and Nimesulide (NS). This indicates the constructed sensor shows a higher current and anti-interference with other foreign molecules. However, this agrees that constructed sensor exposed good selectivity toward detection of NS. Furthermore, the reproducibility study of the constructed ZnFe_2O_4 NPs/GCE was performed via identical DPV analysis. In this study, the four different ZnFe_2O_4 NPs modified GCE, under similar conditions were added in $100 \mu\text{M}$ concentration of NS. As a result, more or less similar currents were observed, shown in Fig. 9C. The corresponding bar diagram also plots between modified electrode vs current as illustrated in Fig. 9D. It indicates the excellent reproducible performance of the constructed sensor towards NS. The repeatability of constructed ZnFe_2O_4 NPs/GCE sensor was evaluated in the presence of $100 \mu\text{M}$ concentration of NS, containing 0.1 M of PBS via DPV analysis. In these studies, the constructed ZnFe_2O_4 NPs/GCE sensor was executed for a consecutive run for 10 cycles and corresponding DPV signals are noted as shown in Fig. 9E. Also, to found a good RSD value exhibit the proposed sensor at 0.97%. In further, the storage stability of the constructed ZnFe_2O_4 NPs/GCE sensor was found on the 1st day, 8th day and 15th day. As a result, to found the loss of current by 0.3% on the 8th day, 0.5 % on the 15th day. It indicates good storage stability of the proposed sensor was shown in Fig. 9F.

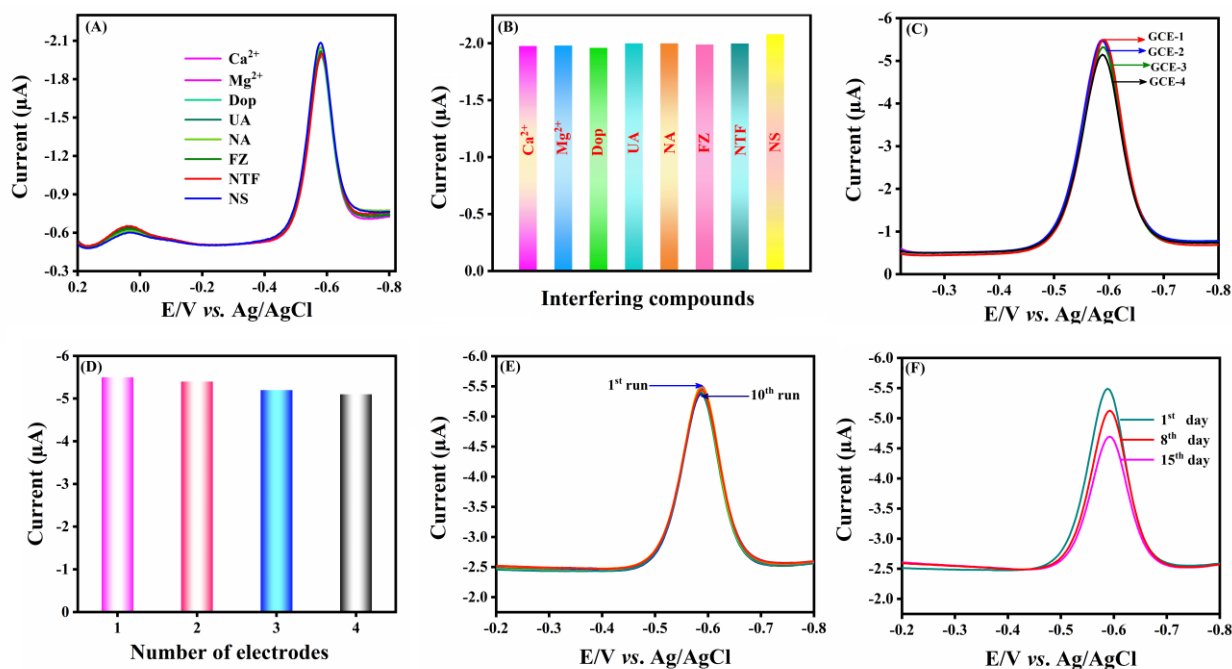


Figure 9. (A) DPV response of NS reduction in the existence of interfering metal ions (Ca²⁺, Mg²⁺, Dop, UA, NA, FZ and NTF). (B) Corresponding bar diagram between current and interfering molecules. (C) DPV depicted reproducibility studied for 100 μM of NS on ZnFe₂O₄ NPs/GCE four different GCE electrodes. (D) Corresponding bar diagram for reproducibility study of four different constructed electrodes. (E) DPV response of repeatability studies for 100 μM NS detection on constructed ZnFe₂O₄ NPs/GCE for 10 consecutive measurements. (F) DPV signal of storage stability studies of 100 μM NS detection on constructed ZnFe₂O₄ NPs electrodes.

3.9. Real sample analysis

The practical utility of constructed sensor was scrutinized via DPV analysis. The detection of NS in real samples are nimesulide tablet and human urine sample. NS tablet was bought from a nearby medical shop and urine samples were collected from healthy humans in Taiwan hospital. The tables are precisely grained using mortar. Then 10 mg of NS grained samples were weighed and diluted with ultrapure water, sonicated for 10 minutes. Further, the impurities were removed via centrifugation. Besides, this test was carryout in N₂ purged 0.1M PBS solution with spiked diluted NS grained solution via standard addition method shown in Fig. 10A. The received recovery values were collected and reported in Table 2. Further, the N₂ purged 0.1 M PBS solution containing a known concentration of NS spiked with diluted urine sample via standard addition method shown in Fig. 10B. Moreover, the recovery values were presented in Table 2. These evident values are demonstrating that, the constructed ZnFe₂O₄ NPs/GCE a sustainable recovery for detection of NS in real samples.

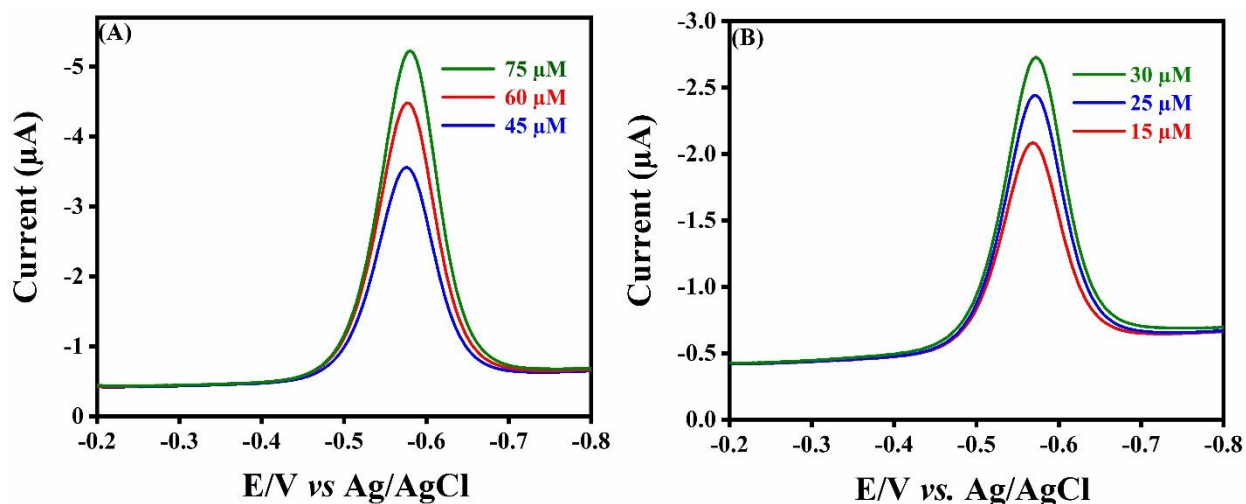


Figure 10. (A) DPV response of NS tablet (B) NS spiked Urine sample.

Table 2. The received recovery values of NS Tablet and human Urine samples.

Sample	Added (μM)	Found (μM)	Recovery (%)
NS Tablet	45	44.7	99.3
	60	59.5	99.1
	75	74.8	99.7
Human urine	15	14.2	94.6
	25	24.8	99.2
	30	29.9	99.6

4. CONCLUSION

In conclusion, we fabricated ZnFe_2O_4 NPs modified electrode exhibits highly sensitive detection of NS sensor. The ZnFe_2O_4 NPs modified electrode has a much lower trace level measurement of NS than previously recorded NS sensors, owing to its unique electrocatalytic activity. The ZnFe_2O_4 NPs fabricated electrode used for specific detection of NS in presence of metal ions, bio-molecules and nitro compounds. The ZnFe_2O_4 NPs modified electrode is thought to be responsible for the high performance and outstanding stability of the NS sensor based on the electrode efficiency. Consequently, the established sensor exhibits a lot of potential for detecting NS in human serum and NS tablet samples. From this study, we recommend that the as-presented ZnFe_2O_4 NPs sensor electrode has applicable for practical pharmaceutical and biological applications.

CONFLICT OF INTEREST

The authors declare no competing financial interest.

ACKNOWLEDGEMENTS

The authors acknowledge the Ministry of Science and Technology (MOST 107-2113-M-027-005-MY3), Taiwan.

References

1. R. Davis, R.N. Brogden, *J. Drug Eval.*, 48 (1994) 431–454.
2. A. Ward, R.N. Brogden, *J. Drug Eval.*, 36 (1988) 732–753.
3. B. Haraoui, J. Pelletier, J. Cloutier, M. Faure, J. M. Pelletier, *J. Arthritis & Rheumatology*, 34(2) (1991), 153–163.
4. D. Canale, I. Scaricabarozzi, P. Giorgi, P. Turchi, M. Ducci, Prof. G. F. Menchini-Fabris, *Andrologia*, 166 (1993) 163–166.
5. N.P. Shetti, S.J. Malode, S.D. Bukkitgar, G.B. Bagihalli, R.M. Kulkarni, S.B. Pujari, K.R. Reddy, *Mater. Sci. Technol.*, 2 (2019) 396–400.
6. A. Alvarez-Lueje, P. Vasquez, L. J. Nunez-Vergara, J.A. Squella, *Anal. Lett.*, 31 (1998) 1173–1184.
7. S. Altino, O. OzcanDursun, *J. Pharm Biomed Anal.*, 22 (2000) 175–182.
8. M. Starek, J. Krzek, *Talanta*, 77 (2009) 925–942.
9. P.T. Kissinger, W. Lafayette, W.R. Heineman, *J. Chem. Educ.*, 60 (1983) 702–706.
10. R.S. Nicholson, *Anal. Chem.*, 37 (1965) 1351–1355.
11. J. Heinze, *Angew. Chem. Int. Ed. Engl.*, 23 (1984) 831–847.
12. R. J. Klingler, J.K. Kochi, *J. Phys. Chem. A.*, 2 (1981) 1731–1741.
13. C. Karupiah, S. Cheemalapati, S.M.Chen, S. Plalanichamy, *Ionics*, 21 (2014) 231–238.
14. F. Wang, S. Hu, *Microchim. Acta*, 165 (2009) 1–22.
15. G.F. Goya, H.R. Rechenberg, *Nanostructured Materials*, 10 (1998) 1001–1011.
16. S. Xiong, S. Ye, X. Hu, F. Xie, *Electrochim. Acta*, 217 (2016) 24–33.
17. C.R. Vestal, Z.J. Zhang, *J. Am. Chem. Soc.*, 125 (2003) 9828–9833.
18. L. Wang, Q. Zhou, F. Li, *phys. stat. sol.*, 382 (2004) 377–382.
19. C. Xiangfeng, Z. Chenmou, *Sens. Actuators B Chem.*, 96 (2003) 504–508.
20. J. S. Jiang, L. Gao, X. L. Yang, J. K. Guo, H. L. Shen, *J. Mater. Sci. Lett.*, 18 (1999) 1781–1783.
21. M.A. Malik, P.O. Brien, *Precursor Chemistry of Advanced Materials*, 9 (2005) 173–204.
22. X. Zhu, C. Cao, S. Su, A. Xia, H. Zhang, H. Li, Z. Li, C. Jin, *Ceram. Int.*, 47 (2021) 15173–15179.
23. R.R. Shahraki, M. Ebrahimi, S.A.S. Ebrahimi, S.M. Masoudpanah, *J. Magn. Magn. Mater.*, 324 (2012) 3762–3765.
24. S. Yu, T. Fujino, M. Yoshimura, *J. Magn. Magn. Mater.*, 256 (2003) 420–424.
25. S.M. Hoque, S. Hossain, S. Choudhury, S. Akhter, F. Hyder, *Mater. Lett.*, 162 (2016) 60–63.
26. A. Kumar, S. Ashoka, P. Malingappa, *J. Environ. Chem. Eng.*, 6 (2018) 6939–6946.
27. L. Lv, P. Cheng, Y. Wang, L. Xu, B. Zhang, C. Lv, J. Ma, Y. Zhang, *Sens. Actuators B Chem.*, 320 (2020) 128384.
28. D. Neravathu, A.R. Paloly, P. Sajan, M. Satheesh, M.J. Bushiri, *Diam. Relat. Mater.*, 106 (2020) 107852.
29. C. Zheng, C. Zhang, L. He, K. Zhang, J. Zhang, L. Jin, *J. Alloys Compd.*, 849 (2020) 156461.
30. Y. Huang, Y. Tang, S. Xu, M. Feng, Y. Yu, *Anal. Chim. Acta*, 1096 (2020) 26–33.
31. L. Ning, X. Guan, J. Ma, M. Wang, X. Fan, G. Zhang, F. Zhang, W. Peng, Y. Li, *J. Alloys*

- Compd.*, 738 (2018) 317–322.
32. P.R. Matli, X. Zhou, D. Shiyu, Q. Huang, *Int. Nano Lett.*, 5 (2015) 53–59.
 33. X. Song, L. Gao, *Langmuir*, 23 (2007) 11850–11856.
 34. J.F. Watts, J. Wolstenholme, *An Introduction to Surface Analysis by XPS and AES*, (2019).
 35. L. Sun, R. Shao, L. Tang, Z. Chen, *J. Alloys Compd.*, 564 (2013) 55–62.
 36. L.R. Hou, L. Lian, L.H. Zhang, G. Pang, C.Z. Yuan, X.G. Zhang, *Adv Funct Mater.*, 25 (2015) 238.
 37. H. Lv, L. Ma, P. Zeng, D. Ke, T. Peng, *J. Mater. Chem.*, 20 (2010) 3665–3672.
 38. H. Song, L. Zhu, Y. Li, Z. Lou, M. Xiao, Z. Ye, *J. Mater. Chem. A*, 3 (2015) 8353–8360.
 39. L. Han, X. Zhou, L. Wan, Y. Deng, S. Zhan, *J. Environ. Chem. Eng.*, 2 (2014) 123–130.
 40. N. Matinise, K. Kaviyarasu, N. Mongwaketsi, S. Khamlich, L. Kotsedi, N. Mayedwa, M. Maaza, *Appl. Surf. Sci.*, 446 (2018) 66–73.
 41. X. Wu, Z. Wei, L. Zhang, X. Wang, H. Yang, J. Jiang, *J. Nanomater.*, 2014 (2014).
 42. A.R.C. Bredar, A.L. Chown, A.R. Burton, B.H. Farnum, *ACS Appl. Energy Mater.*, 3 (2020) 66–98.
 43. M.M. Walczak, D.A. Dryer, D.D. Jacobson, M.G. Foss, N.T. Flynn, *J. chem. Educ.*, 74 (1997) 1195–1197.
 44. E. LAVIRON, *J. Electroanal chem.*, 112 (1980) 1-9.
 45. F. Agin, V. Serdaroglu, *Turk J Pharm Sci.*, 13 (2016) 335–341.
 46. C. Wang, X. Shao, Q. Liu, Q. Qu, G. Yang, X. Hu, *J. Pharm. Biomed. Anal.*, 42 (2006) 237–244.
 47. J. Zhang, X. Tan, D. Zhao, S. Tan, Z. Huang, Y. Mi, Z. Huang, *Electrochim. Acta*, 55 (2010) 2522–2526.
 48. O.W. Lau, S.F. Luk, Y.M. Cheung, *Analyst*, 114 (1989) 1047–1051.
 49. Z. Jin-lei, T. Xue-cai, Z. Dan-dan, T. Sheng-wei, L. Li, W. Lin, H. Zeng-wei, *Chem. Res. Chinese Univ.*, 27 (2011) 566–569.